

Anisotropy tuning with the Wilson flow

Szabolcs Borsányi,^a Stephan Dürr,^{a,b} Zoltán Fodor,^{a,b,c} Sándor D. Katz,^c Stefan Krieg,^{a,b} Thorsten Kurth,^a Simon Mages,^d Andreas Schäfer,^d and Kálmán K. Szabó^a

^a*Bergische Universität Wuppertal, Gausstr. 20, D-42119 Wuppertal, Germany.*

^b*Jülich Supercomputing Centre, Forschungszentrum Jülich, D-52425 Jülich, Germany.*

^c*Institute for Theoretical Physics, Eötvös University, H-1117 Budapest, Hungary.*

^d*Universität Regensburg, Universitätsstr. 31, D-93053 Regensburg, Germany*

ABSTRACT: We use the Wilson flow to define the gauge anisotropy at a given physical scale. We demonstrate the use of the anisotropic flow by performing the tuning of the bare gauge anisotropy in the tree-level Symanzik action for several lattice spacings and target anisotropies. We use this method to tune the anisotropy parameters in full QCD, where we also exploit the diminishing effect of a well chosen smearing on the renormalization of the fermion anisotropy.

KEYWORDS: Lattice QCD, anisotropic lattices

Contents

1	Introduction	1
2	Wilson flow on anisotropic lattices	2
3	Scale and gauge anisotropy from the Wilson flow	3
4	Comparison to Klassen’s method	6
5	Universality of the anisotropic flow	9
6	Parameter tuning in the quenched case	11
7	Fermion anisotropy	12
8	Parameter tuning with dynamical quarks	14
9	Conclusions	16
A	Lattice actions	16

1 Introduction

Lattice QCD provided full, ab-initio answers for many questions of hadronic physics e.g. the light hadron spectrum [1]. Nevertheless, there are many questions, which are very difficult to answer. One characteristic example is the ordering of the nucleon spectrum. In principle we have techniques to understand ordering questions in spectrums (actually few groups’ results indicate a proper ordering for the nucleon states [2, 3]). The major issue in this example is to obtain a good signal for the excited states with fine enough lattice spacing. In order to minimize finite volume effects (by having large enough spatial extensions) with fine enough spacings in the temporal direction one might take larger lattice spacings in the spatial directions (a_s) than in the temporal one (a_t). These asymmetric lattices are obtained by anisotropic bare couplings.

Anisotropic lattice actions have a long history both for pure gauge theories and for gauge plus fermionic systems.

In the quenched approximation anisotropic actions have been used to determine the glueball spectrum [4], to study heavy hybrids [5, 6] and also for charmonium states [7–9]. The mostly advocated technique to determine the lattice spacing asymmetry is based on the comparison of spatial-spatial and spatial-temporal Wilson loops. A robust method for the determination of the gauge anisotropy is even more important in dynamical simulations, where less statistics are available for tuning.

For our purposes this dynamical case is the more important one. Dynamical simulations have been done for the first time by the CP-PACS collaboration using the Iwasaki gauge and clover improved fermion action [10]. The TrinLat collaboration used a Symanzik-improved gauge action and a Wilson fermion action with a Hamber-Wu term [11]. Edwards et al. used a clover-improved fermionic action with stout-link smearing (in the spatial directions only) and a Symanzik-improved gauge action [12]. The latter is probably the most extensively used action today and led to several interesting results (e.g. light hadron [13] or excited and exotic charmonium [14] spectroscopy). Another important application is to study spectral functions at non-vanishing temperatures [15]. In this case the many points of the meson correlators in the temporal direction helps to determine the spectral function when one uses the Maximum Entropy Method (MEM).

In the present paper we suggest an anisotropic action, which we plan to use in our non-vanishing temperature studies. It is very similar to the isotropic action, which we used in the the Budapest-Marseille-Wuppertal collaboration for determining e.g. the light hadron spectrum [1], quark masses [16, 17] or the transition temperature [18]. After defining the action we show how to set the anisotropy parameters. In the interacting discretized theory the anisotropy parameters in the action (bare anisotropies) differ from the observed asymmetry, which is usually determined through the comparison of time and space-like correlation lengths. Ignoring the radiative corrections to the anisotropy parameters will introduce discretization errors that depend on the logarithm of the lattice spacing, making a continuum extrapolation practically impossible. Instead of the most popular choice, using Wilson loops to determine the a_s/a_t asymmetry in the gauge sector, we apply the Wilson flow. In the fermionic sector the mass ratios of the pseudoscalars are used.

2 Wilson flow on anisotropic lattices

In the continuum the Yang-Mills or Wilson flow is the solution of the differential equation

$$\frac{dA_\mu}{d\tau} = D_\nu F_{\nu\mu} \quad (2.1)$$

for the gauge field $A_\mu(x, \tau)$ supplemented with an initial condition at $\tau = 0$. The variable τ parametrizing the flow has a dimension of length squared. Expectation values of operators along the Wilson flow have been a subject to recent studies in the SU(N) theory as well as in full QCD. It was shown [19] that for any $\tau > 0$ time the field defined by the flow is renormalized, no UV divergences appear to any order in perturbation theory.

On the lattice the flow was investigated by Luscher [20] primarily to study the behaviour of gauge field updating algorithms. It was considered earlier by Narayanan and Neuberger [21] in a different context. The discretization of the flow equation gives

$$\frac{dU_\mu}{d\tau} = X_\mu(U)U_\mu \quad (2.2)$$

where X_μ is the generator of the stout smearing transformation [22]:

$$X_\mu(x, \tau) = \mathcal{P}_A \left[\sum_{\pm\nu \neq \mu} \rho_{\mu\nu} U_\nu(x, \tau) U_\mu(x + \nu, \tau) U_\nu^\dagger(x + \mu, \tau) U_\mu^\dagger(x, \tau) \right], \quad (2.3)$$

with \mathcal{P}_A operator projecting onto traceless, anti-hermitian matrices, and in this case the smearing parameters are $\rho_{\mu\nu} = 1$. The flow variable τ is made dimensionless using the second power of the lattice spacing (ie. $\tau/a^2 \rightarrow \tau$ when discretizing the flow). The simplest way of implementing the Wilson flow is to make successive stout smearing steps on a gauge field configuration with a small enough smearing parameter. Note, that there exist sophisticated integrators for the flow like the third-order method introduced in [23].

It was also realized [23], that the Wilson flow provides a length scale, called $\sqrt{t_0}$, which can be used to set the scale in lattice simulations. In [24] we derived another scale from the Wilson flow, w_0 . It is defined by the following equation:

$$\left[\tau \frac{d}{d\tau} \tau^2 \langle E(\tau) \rangle \right]_{\tau=w_0^2} = 0.3, \quad (2.4)$$

where $\langle E(\tau) \rangle$ is the quantum expectation value of the Yang-Mills action density

$$E(\tau) = \frac{1}{4} \sum_x F_{\mu\nu}^2(x, \tau). \quad (2.5)$$

This new scale was shown to be advantageous by many means: it can be measured with high precision on the lattice, its definition is free from fitting and extrapolation, it has only small quark mass dependence and it is not sensitive to the details of the lattice discretization. Since w_0 is not directly measurable in experiments, in [24] we also calculated w_0 in physical units using previous lattice QCD data and obtained $w_0 = 0.1755(18)(04)$ fm.

In the following let us consider an anisotropic lattice, ie. let the ratio of lattice spacings in the spatial and temporal directions be different. The observed anisotropy of the gauge configurations we denote by $\xi_g = a_s/a_t$. Discretizing the continuum flow equation on this lattice yields the same as Equations (2.2) and (2.3). The flow variable is now made dimensionless by the spatial lattice spacing (ie. $\tau/a_s^2 \rightarrow \tau$). The difference to the isotropic case is, that the smearing coefficients have to be chosen as $\rho_{i4} = \xi_g^2$ and $\rho_{ij} = \rho_{4i} = 1$ in order to obtain the correct flow equation in the continuum limit.

In a non-interacting theory there is only one anisotropy parameter: ξ_g , which also enters into the lattice action. When an interacting theory is discretized on an anisotropic lattice, the action is written in terms of bare anisotropy parameters (eg. $\xi_g^{(0)}$ bare gauge anisotropy) and unrenormalized fields. The bare parameters describe the theory on the scale of the lattice spacing. ξ_g will then be termed as renormalized gauge anisotropy, it can be measured from gauge observables on the physical scale. Since for any time $\tau > 0$ the gauge field along the Wilson flow is already renormalized, we expect, that the anisotropy parameter in the Wilson flow is the renormalized gauge anisotropy ξ_g .

3 Scale and gauge anisotropy from the Wilson flow

Similarly to the isotropic case the Wilson flow offers a convenient scale setting procedure on the anisotropic lattice, too. Additionally it also offers a way to determine the renormalized gauge anisotropy. We write the spatial and temporal contribution of the action density in

Equation (2.5) separately as

$$E_{ss}(\tau) = \frac{1}{4} \sum_{x, i \neq j} F_{ij}^2(x, \tau), \quad (3.1)$$

$$E_{st}(\tau) = \frac{1}{2} \sum_{x, i} F_{i4}^2(x, \tau). \quad (3.2)$$

In physical units the expectation values of these two parts are equal. Since for any $\tau > 0$ these operators are renormalized, they offer a definition for the renormalized gauge anisotropy: $\xi_g^2 = a_s^2/a_t^2$ can be defined as the ratio of the field strength tensors in lattice units at some point along the flow $\langle a_s^4 E_{ss}(\tau) \rangle / \langle a_s^2 a_t^2 E_{st}(\tau) \rangle$. From now on we work in lattice units, ie. $a_s^4 E_{ss} \rightarrow E_{ss}$, $a_s^2 a_t^2 E_{st} \rightarrow E_{st}$, $\tau/a_s^2 \rightarrow \tau$ and $w_0/a_s \rightarrow w_0$. Instead of working with the field strength tensors directly, we will consider the derivative of these tensors along the flow, ie. instead using $\langle E_{ss} \rangle / \langle E_{st} \rangle$ we define the ratio

$$R_E = \left[\tau \frac{d}{d\tau} \tau^2 \langle E_{ss}(\tau) \rangle \right]_{\tau=w_0^2} \bigg/ \left[\tau \frac{d}{d\tau} \tau^2 \langle E_{st}(\tau) \rangle \right]_{\tau=w_0^2}. \quad (3.3)$$

Let us now turn to our definition of the w_0 -scale and the renormalized anisotropy using the Wilson-flow. We use the spatial part of Equation (2.4) to define the w_0 -scale

$$\left[\tau \frac{d}{d\tau} \tau^2 \langle E_{ss}(\tau) \rangle \right]_{\tau=w_0^2} = 0.15, \quad (3.4)$$

and we define the renormalized gauge anisotropy through the R_E ratio:

$$\xi_g^2 = R_E, \quad (3.5)$$

analogously to $\xi_g^2 = \langle E_{ss} \rangle / \langle E_{st} \rangle$. The calculation of R_E itself requires the knowledge of the anisotropy ξ_g which enters into the discretized flow equation (2.2). Therefore Equations (3.4) and (3.5) become a set of coupled equations for the unknown lattice anisotropy and w_0 -scale.

To solve these equations, and find ξ_g for an ensemble of gauge configurations with unknown anisotropy one evaluates the flow with various anisotropy parameters $\rho_{i4} = \xi_w^2$ and $\rho_{ij} = \rho_{4i} = 1$ in Equation (2.3). For each ξ_w one first locates the flow time, where Equation (3.4) holds and then calculates the ratio in Equation (3.3). Then one searches for the solution of the equation

$$R_E(\xi_w) / \xi_w^2 = 1, \quad (3.6)$$

which provides the gauge anisotropy $\xi_g = \xi_w$.

The procedure of measuring the gauge anisotropy is illustrated on a quenched ensemble generated with plaquette action with bare gauge anisotropy parameter $\xi_g^{(0)} = 2.46$ (see the Appendix for the definition of the action). Here we use a lattice size of $28^3 \times 84$. Figure 1 shows $\tau d\tau^2 \langle E_{ss} \rangle / d\tau$ and $\tau d\tau^2 \langle E_{st} \rangle / d\tau$ along the Wilson flow two different Wilson flow anisotropies. In the figure $\langle E_{st} \rangle$ is rescaled by ξ_w^2 . $\langle E_{st} \rangle$ and $\langle E_{ss} \rangle$ are in the same units only if $\xi_g = \xi_w$, but at this point we do not yet know ξ_g .

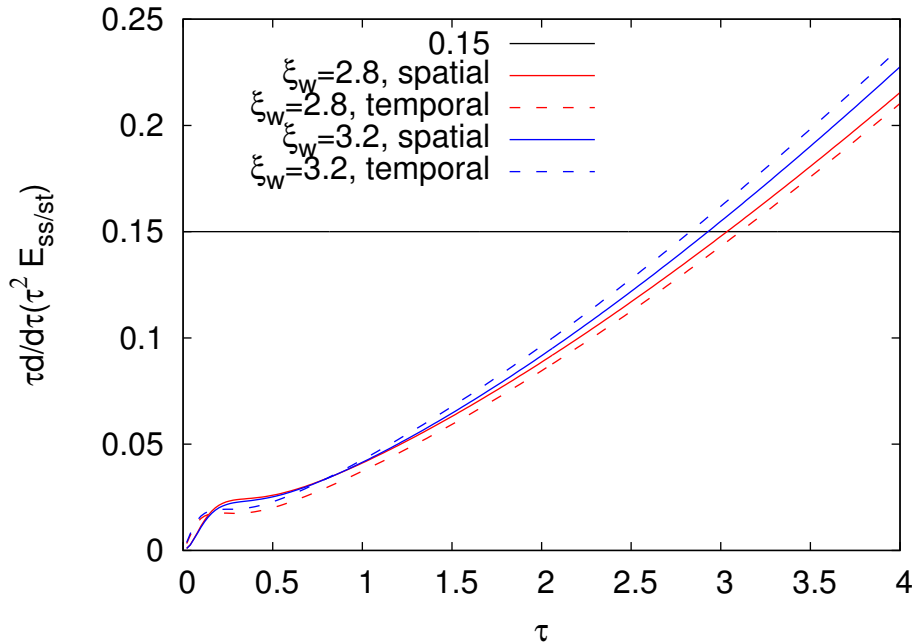


Figure 1. The derivative of the action density along the anisotropic Wilson-flow at two different anisotropy parameters, $\xi_w = 2.8$ and 3.2 . The renormalized anisotropy is between these two values. The temporal action density has been multiplied by ξ_w^2 , so that the spatial and temporal curves are similar in magnitude. Notice that the temporal and spatial parts switch order between the two flow anisotropies. In Figure 2 we will define the renormalized gauge anisotropy as ξ_w at which the two curves coincide at $\tau = w_0^2$. (Parameters: $\beta = 6.1$, plaquette action with a bare anisotropy of $\xi_g^{(0)} = 2.46$.)

Figure 2 explains the determination of ξ_g . We integrated the Wilson flow on the same ensemble several times, each time with a different ξ_w parameter. The left hand side of Equation (3.6) is plotted as a function of ξ_w . In each case the ratio was defined at the respective $\tau = w_0^2$ scale of the corresponding flow. The self-consistency condition (3.6) translates in the lower plot to the crossing of the dotted line at 1.0. Where this occurs defines the actual gauge anisotropy $\xi_g = \xi_w$. The interpolation between the analyzed flows brings in no difficulty, the dependence on ξ_w is remarkably linear. For this particular ensemble we find $\xi_g = 2.958(3)$ for the gauge anisotropy and $w_0/a = 1.730(1)$ for the w_0 -scale in spatial lattice units. This converts to a lattice spacing of $a_s \approx 0.102$ fm.

Let us close this section with a remark. We use the derivatives of the field strength tensors in Equation (3.3) and in Equation (3.4). We found that although the plain ratio $\langle E_{ss} \rangle / \langle E_{st} \rangle$ could be an equally correct measure of anisotropy, its scaling features are sub-optimal, even more so as it was in the case of the scale setting. We checked on several examples that as $\tau \rightarrow \infty$ the ratio $\langle E_{ss}(\tau) \rangle / \langle E_{st}(\tau) \rangle$ does indeed converge to $R_E(\tau)$, but the $R_E(\tau)$ saturates much faster with growing flow time τ as the simpler ratio. In fact, it is not necessary to define the anisotropy through the $\tau \rightarrow \infty$ asymptotic behaviour, one may define it at any fixed physical scale, like $\tau = w_0$.

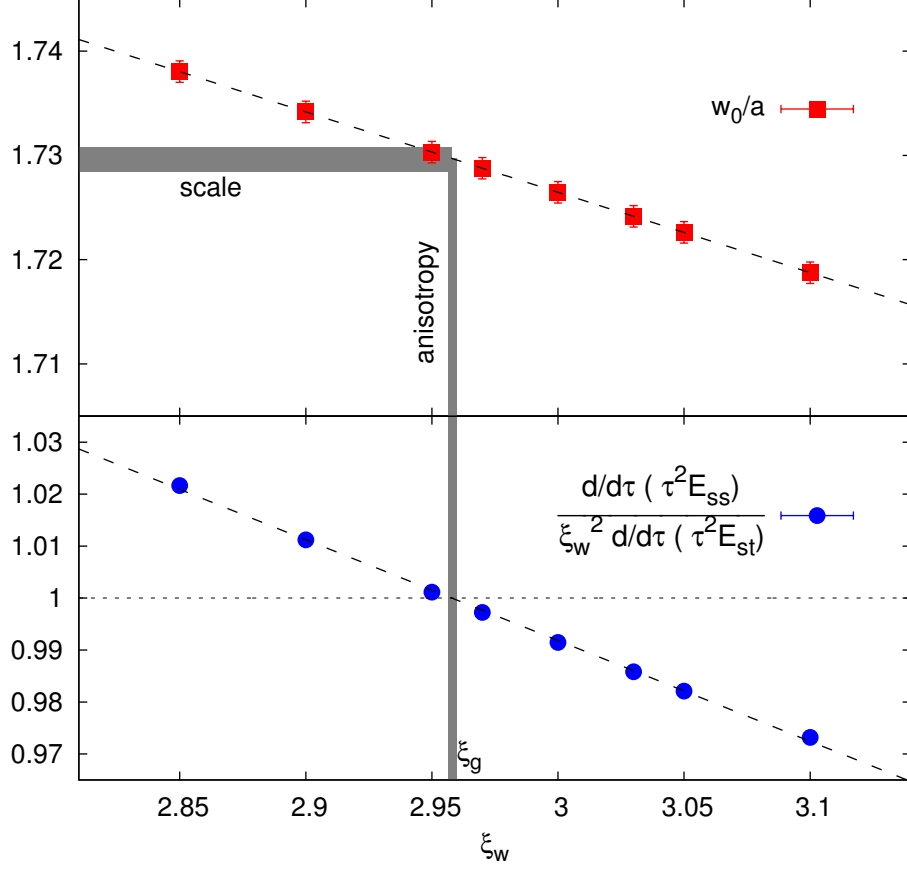


Figure 2. The determination of the gauge anisotropy from the Wilson flow. The same set of gauge configurations have been analyzed with various ξ_w parameters. For each ξ_w the (spatial) w_0 scale was determined through Equation (3.4). From each flow, the ratio R_E in Equation (3.3) was evaluated at the respective scale $\tau = w_0^2$. We define the (renormalized) gauge anisotropy ξ_g as the ξ_w flow anisotropy parameter at which the ratio (R_E) of the field strength derivatives is equal to ξ_w^2 . In this plot we divided this ratio by the square of the actually used ξ_w , so that the fulfilment of the defining condition is marked by a unit value of this combination. We then interpolate w_0/a to the newly defined $\xi_w = \xi_g$ point and use it as a scale setting observable.

4 Comparison to Klassen's method

Our next task is to compare the continuum scaling behaviour of our new gauge anisotropy determination with an existing method. In the literature the gauge anisotropy is usually calculated from ratios of Wilson loops:

$$R_{ss}(x, y) = \frac{W_{ss}(x, y)}{W_{ss}(x + 1, y)}, \quad (4.1)$$

$$R_{st}(x, t) = \frac{W_{st}(x, t)}{W_{st}(x + 1, t)} \quad (4.2)$$

the so-called Klassen-ratios [9]. The anisotropy is obtained from requiring, that for a given x and y the two ratios are equal at $t = y \cdot \xi_g$:

$$R_{ss}(x, y) = R_{st}(x, y \cdot \xi_g). \quad (4.3)$$

In practice one averages the so obtained ξ_g 's for different x and y values, for which the ratios are already in the asymptotic regime. The major problem with this method is that one has to go beyond a few lattice spacings both for x and y to avoid excited state contributions. However, measuring these ratios becomes notoriously difficult as the size of the Wilson-loop is increased. A further difficulty arises for non-integer ξ_g , since the condition in Equation (4.3) requires the interpolation of the ratio (4.2). Since the ratio exists for integer t values only this interpolation is always ambiguous.

For the comparison we again use the plaquette action, where Klassen's tuned bare anisotropies are known to reproduce $\xi_g \approx 3$. In addition to the data in Figure 2 we generated three more ensembles in the β range [5.8,6.2]. We calculated ξ_K from Equation (4.3). The determination of ξ_K includes a simultaneous polynomial fit of both ratios ($R_{ss}(x, y)$ and $R_{st}(x, \xi_K y)$) for each x , with the $y > x$ restriction. ξ_K was defined by the minimum of the global χ^2 of the fit for any given x . As a last step, we performed an asymptotic fit in the Wilson loop size parameter x .

For our Wilson-flow based anisotropy we integrated the Wilson flow several times with various ξ_w parameters and determined ξ_g . The solution of Equation (3.6) requires the interpolation of the data obtained with various flow parameters. In contrast to the case of the Klassen ratios, here the interpolation can be made arbitrarily precise by increasing the number of ξ_w parameters at which the flow is integrated. The point in using the Wilson-flow (or continuous smearing) was in fact to select a scale of interest in both directions independently, and without being restricted to integer multiples of the lattice spacing. The absence of delicate fits enables a great level of automatization.

β	5.8	6.0	6.1	6.2
$\xi_g^{(0)}$	2.38	2.44	2.46	2.49
lattice	$24^3 \times 72$	$24^3 \times 72$	$24^3 \times 48$	$32^3 \times 96$
ξ_g	2.917(2)	2.942(5)	2.958(3)	2.979(1)
ξ_K	2.91(4)	3.01(2)	2.99(3)	3.01(2)
w_0	1.006(1)	1.465(1)	1.730(1)	2.015(3)

Table 1. Ensembles used to compare our ξ_g to ξ_K .

Table 1 and Figure 3 summarizes the result of the comparison. We see deviations between the two anisotropy definitions on the percent level. The errors on ξ_K are larger than on ξ_g , and some of the systematics are not controlled to our satisfaction. Different definitions for the gauge anisotropy do not need to agree for any one ensemble, but in the continuum limit. Figure 3 shows the ratio of ξ_K/ξ_g as a function of a^2 . If the coarsest lattice is not included in the extrapolation, the continuum limits are compatible.

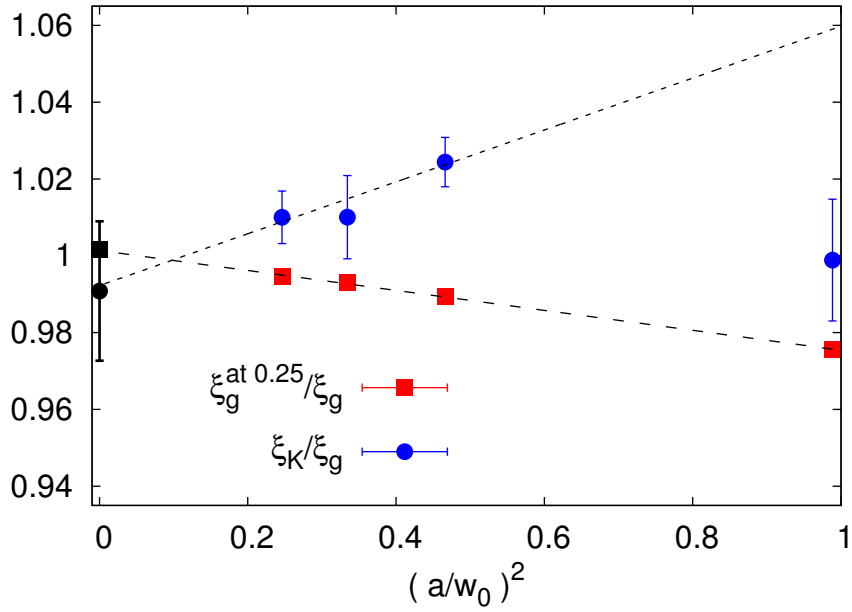


Figure 3. The ratio of various gauge anisotropy definitions extrapolate to one in the continuum. Blue circles: the anisotropy from the Klassen ratios divided by our definition. Red squares: an other possible definition with 0.25 on the right hand side of Equation (3.4), again plotted relative to our ξ_g .

Figure 3 shows an other comparison, too. A clear point of ambiguity in our scheme is the choice of the scale at which R_E and through that ξ_g is defined. Equation (3.4) defines the w_0 scale for anisotropic lattices, but instead of the constant 0.15 any other positive number could stand there. This constant tunes whether the anisotropy is renormalized at 0.1755 fm or at a different length scale. For these ensembles we determined the gauge anisotropy with 0.25 on the right hand side of the scale definition, resulting in a $\approx 21\%$ increase in the renormalization scale. In Fig 3 we show in red the ratio of this alternative result to our original definition. We find that the continuum extrapolation of the ratio very strictly follows an a^2 behaviour and hits one in the continuum to per mill accuracy.

In principle, any constant in Equation (3.4) results in a valid definition, although the choice of this constant may influence the range of available lattice spacings: on very fine lattices the flow time will grow unpractically long, and on the other side, the coarse lattices may be outside of the scaling regime. We made our choice to select the phenomenologically relevant range of applicability.

A crucial ingredient in our definition is the use of a physical scale. This is in contrast to more conventional schemes, where one calculates the anisotropy at a scale fixed in lattice units. Then one extrapolates the scale to the far infrared, as much as possible. It is technically feasible to fix the scale of anisotropy renormalization in lattice units, say $\tau = 9a^4$. We found, however, that although such a scheme deviates from our discussed

definition on the percent level only, the discretization errors do not shrink as $\sim a^2$. The discretization ambiguities in our final definition, which is based on the w_0 scale, do indeed scale as $\sim a^2$ as we present in the next Section.

5 Universality of the anisotropic flow

So far we have only considered the isotropic Wilson flow, discretized on an anisotropic lattice. Here we discuss the opposite situation, where the Wilson flow is anisotropic in the physical sense.

Thinking of the Wilson-flow as an UV-filter the flow equation's anisotropy parameter ξ_w sets the ratio of the smearing radii. In an isotropic setting at flow time τ lattice modes outside of a four-sphere in momentum space of a radius ($\sim \tau^{-1/2}$) are suppressed. The anisotropic Wilson flow suppresses modes with momenta outside of a four-ellipsoid. If ξ_w is set to the gauge anisotropy defined at the scale $\sim \sqrt{\tau}$, i.e. $\xi_w = \xi_g$, then the radii of this ellipsoid will be equal in physical units, and the flow will be isotropic in the physical sense. Only if the flow is isotropic in this physical sense, can one assume that the temporal and spatial parts of the action densities (and their derivatives) are equal in physical units, i.e. $E_{ss}/E_{st} = \xi_g^2$ or $R_E = \xi_g^2$.

Setting ξ_w independently of the actual anisotropy ξ_g one can easily work out the tree-level formulas for the action densities at linear order in $\xi_w^2 - 1$

$$E_{ss}^{\text{tree level}}(\tau) = \frac{g^2(N_c^2 - 1)}{256\pi^2\tau^2} [3 - (\xi_w^2/\xi_g^2 - 1)] \quad (5.1)$$

$$E_{st}^{\text{tree level}}(\tau) = \frac{1}{\xi_g^2} \frac{g^2(N_c^2 - 1)}{256\pi^2\tau^2} [3 - 2(\xi_w^2/\xi_g^2 - 1)] \quad (5.2)$$

where N_c is the number of colors. One may use running coupling constant g evaluated at $\mu = \sqrt{8\tau}$ scale [23], though the consistent treatment of the running coupling would require higher orders in the E 's perturbative expansion.

We do not expect our lattice data to be in the perturbative regime where these formulae apply. We quoted these continuum results to emphasize that flows with a non-trivial anisotropy ξ_w can be studied independently of the anisotropy of the lattice. Actually the simplest way to study the anisotropic flow is to use isotropic configurations, where $\xi_g = 1$ is granted.

Encouraged by the finiteness of the perturbative formulae, which is valid for any ξ_w/ξ_g , we calculate the ratio R_E/ξ_w^2 in the non-perturbative regime with simulations of the SU(3) theory. Our hypothesis is that R_E/ξ_w^2 has a well defined continuum limit for any ξ_w/ξ_g .

To collect numerical evidence on our hypothesis we calculated the R_E ratio at several ξ_w parameters. This enabled us to know ξ_g as well. In Figure 4 we plot ξ_g/ξ_w as a function of R_E/ξ_w^2 . If the flow is isotropic in physical units, both ratios are equal to one. The curve, (which is very close to linear), is shown for several lattice spacings, two gauge actions, and three renormalized anisotropies. All show the same result up to tiny cut-off effects. To linear order the curve can be parametrized as

$$\xi_g/\xi_w = 1 + 1.71(R_E/\xi_w^2 - 1). \quad (5.3)$$

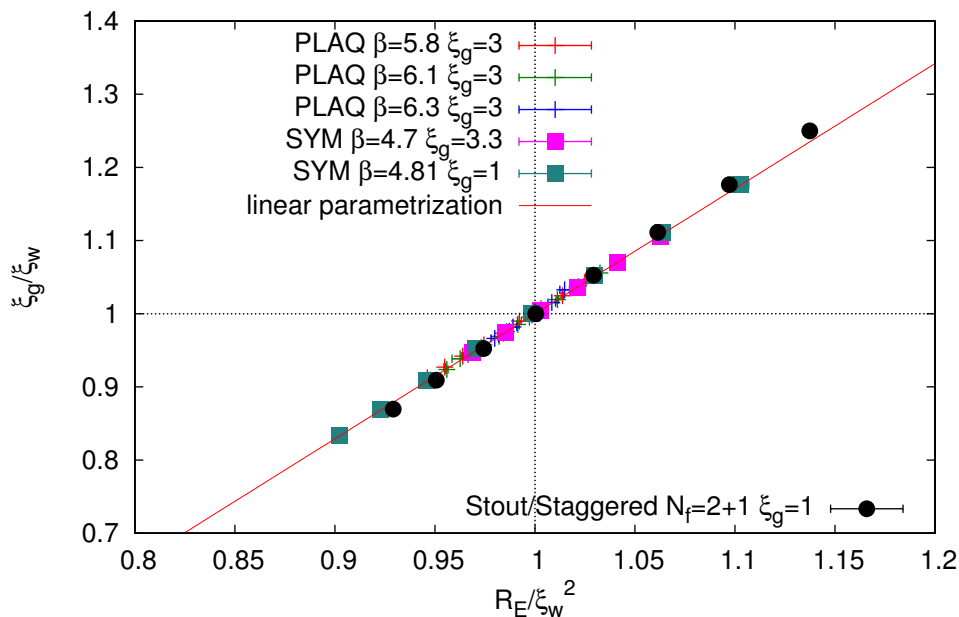


Figure 4. The ratio of anisotropies ξ_g/ξ_f and R_E/ξ_w^2 are connected by a universal function. The staggered data set indicates that the effect of unquenching is rather mild for this observable.

This confirms our assumption that the universality of R_E/ξ_w^2 is not restricted to the case where $\xi_g = \xi_w$ and thus the flow is isotropic in physical units.

Especially in full QCD, the Wilson flow analysis is significantly cheaper than the generation of independent configurations, and it is normally not an obstacle to calculate R_E at several ξ_w parameters. In some cases, like quenched QCD, the flow integration may seem expensive. The determination of ξ_g can then be greatly simplified if the relation is known between R_E , ξ_w and ξ_g . One then tries to guess ξ_g to, say, 10% accuracy (the typical size of radiative corrections to the anisotropy with improved actions), and measures R_E . Figure 4 can then be used to determine ξ_g/ξ_w and thus also ξ_g .

The universality is not guaranteed between quenched and full QCD. Nevertheless we find that the effect of the quarks on this particular relation is mild. To illustrate this we plot a staggered data set ($a = 0.12 \text{ fm}$, physical quark masses, 2+1 flavors). Though not compatible with the quenched data, it is remarkably close.

The basic tool in our tuning procedure, the Wilson flow, was also advertised as “gradient flow” in Reference [19]. This name refers to the fact that the generator of the stout smearing in Equation (2.3) is the gradient of the widely used plaquette gauge action: $X = -\partial S_g/\partial U$. In Reference [24] we have already given up on this correspondence by using the gluonic flow equation in full QCD. We also provided numerical evidence for the irrelevance of the improvement terms in the gauge action that is used to construct the flow equation. The flow based on the derivative of the tree-level Symanzik action gave precisely the same continuum limit, as the simpler flow based on the plaquette action. This was

checked on configurations generated using the Wilson as well as the Symanzik gauge action, with or without quarks.

Here we manifestly break the concept of the “gradient flow” by using the renormalized anisotropy in the flow equation, in contrast to the action where the bare anisotropy is used. In this presentation the Wilson flow is part of the observable, that selects a particular macroscopic scale in both time and spacelike directions. Our method is expected to work independently on the details of the action that was used to generate the configurations. If we used $\xi_g^{(0)}$ in the Wilson flow, R_E gave very different anisotropies, that are quite incompatible with ξ_K in Figure 1. Actually Figure 4 can also be used to predict this behaviour: Substituting ξ_w by $\xi_g^{(0)}$ in the parametrization (5.3) and performing a linear approximation in $\xi_g^{(0)}/\xi_g^2 - 1$ one finds $R_E/\xi_g^2 \approx 1 + 0.71 \left((\xi_g^{(0)}/\xi_g)^2 - 1 \right)$. Using the numbers in Table 1 we find that $\sqrt{R_E}$ is about 12% lower than with the correct definition.

6 Parameter tuning in the quenched case

In the pure gluonic theory there is only one extra bare parameter that is induced by the 3+1-anisotropy. In this Section we tune this bare parameter such that ξ_g is equal to a predefined target value. Keeping ξ_g constant over a range of lattice spacings is a particularly important ingredient of a continuum extrapolated lattice result.

In the course of tuning one could determine ξ_g for several bare anisotropy parameters (ξ_0), and find the preferred choice through interpolation. The procedure is somewhat simplified in the sense that for every ξ_0 the Wilson flow is integrated once only. In fact, we may use the target anisotropy $\xi_w = \xi_g$ for all bare anisotropies. The configurations, that are generated on the fly for the flow integration need not be stored. Again, R_E/ξ_g^2 is measured and interpolated in ξ_0 . The equation $R_E = \xi_g^2$ locates the point where ξ_0 is accepted.

In this Section we tabulate the tuned anisotropies that we determined for the tree-level Symanzik gauge action. For a limited number of gauge couplings References [25, 26] gives the tuned bare anisotropies for this action as well as the Iwasasaki and DBW2 actions, though the main focus there was to establish the perturbative regime. With our method we can give $\xi_g^{(0)}$ with sub-percent precision, accompanied with the scale setting. Since the anisotropy is defined on the w_0 scale, this length scale has to be resolved by the lattice and contained by the box. This condition, however, rules out the discussion of perturbative gauge couplings.

In our set of simulations the lattice box size was always larger than $8w_0$. The aspect ratio of the lattice matched the renormalized anisotropy. The quenched configurations were generated on the QPACE machine with a separation of 50 updates (each consisting of 1 heatbath + 4 overrelaxation sweeps) between measurements. $\xi_g^{(0)}$ was sought in four or more points in the range $\pm 20\%$ around the estimated bare anisotropy. We used a quadratic fit for the interpolation in $\xi_g^{(0)}$. Our results are given in Table 2.

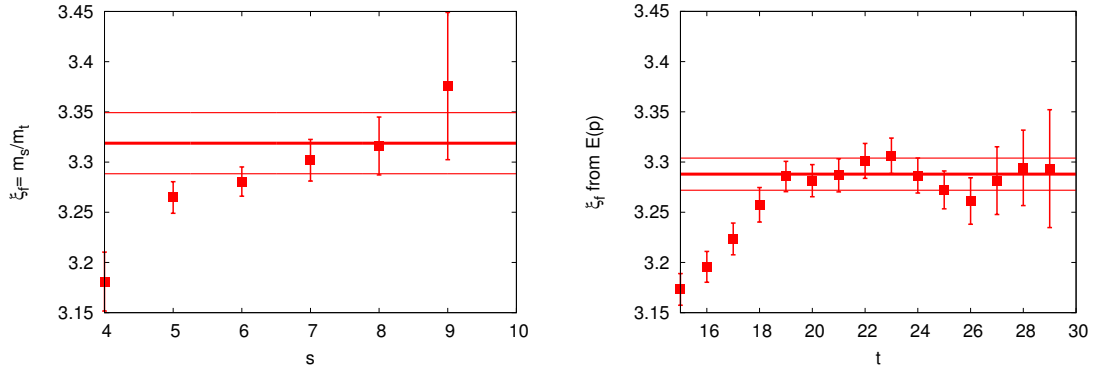


Figure 5. Left: Fermion anisotropy determined from Equation (7.1). Right: Fermion anisotropy determined from Equation (7.3).

7 Fermion anisotropy

If quarks are considered on an anisotropic lattice, then a bare anisotropy parameter $\xi_f^{(0)}$ has to be introduced in the quark action and tuned as the lattice spacing is changed. We use a clover improved Wilson quark action for this study, the definition can be found in Equation (A.3). The anisotropy of the lattice measured from observables, that are built up from the quarks, is called fermion anisotropy, ξ_f . The bare parameters of the action have to be tuned such, that the renormalized anisotropies, ξ_f and ξ_g are equal.

For the fermion anisotropy ξ_f one usually extracts the masses from the asymptotic decay of a hadron correlator in the spatial and temporal directions:

$$m_s/m_t = \xi_f, \quad (7.1)$$

where m_s and m_t are the masses in the spatial and temporal directions. In practice we consider the standard effective masses in both directions, and for each spatial separation s we solve the equation

$$m_s(s)/m_t(s \cdot \xi_f(s)) = \xi_f(s), \quad (7.2)$$

for $\xi_f(s)$, which we call “effective anisotropy”. For the solution the temporal mass is interpolated to non-integer arguments. The fermion anisotropy is then defined as the plateau of the effective anisotropy as $s \rightarrow \infty$. Alternatively one can also measure the hadron energy for nonzero momenta from the temporal hadron correlator, and define ξ_f as

$$E_t^2(p) = m_t^2 + \frac{p^2}{\xi_f^2}. \quad (7.3)$$

This can be done for each separation in time, so one obtains an effective anisotropy plot again. The two definitions might differ in lattice artefacts, that are proportional to the lattice spacing.

We illustrate these two methods on quenched configurations generated with tree level improved Symanzik gauge action. The parameters are

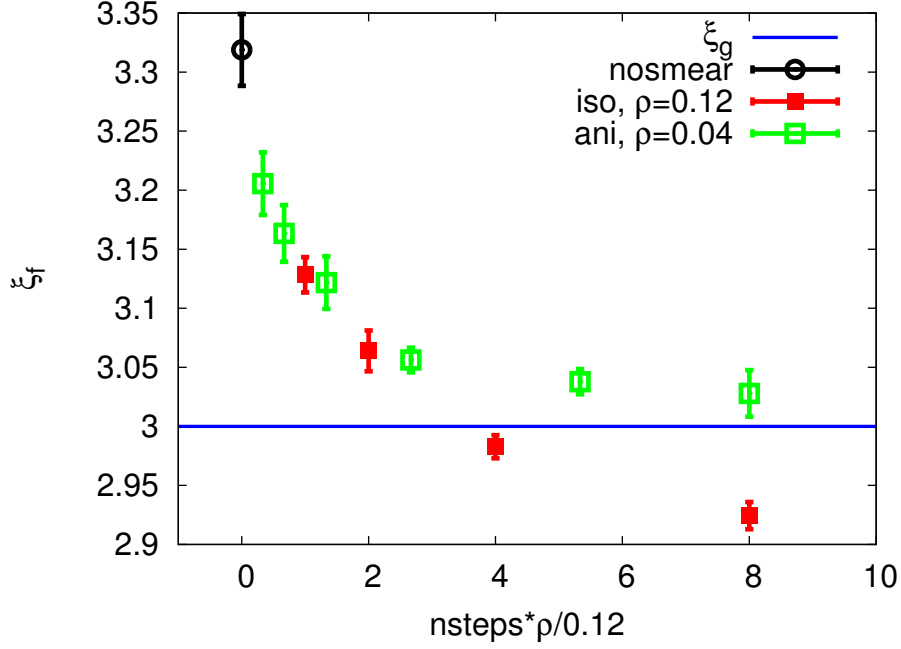


Figure 6. The renormalized fermion anisotropy as the function of smearing steps for “isotropic” and “anisotropic” stout smearing. In the latter case the number of steps is scaled by a factor 3.

lattice size	$20^3 \times 60$
β	4.46
$\xi_g^{(0)}$	2.674

We obtain for $w_0/a_s = 1.379(2)$ and $\xi_g = 2.999(8)$. The hadron, we choose for the ξ_f determination, is the pseudoscalar meson with the mass set approximately to $m_s = 0.25$. The bare fermion anisotropy is set to $\xi_f^{(0)} = 3$. The figures correspond to 0.13 fm spatial lattice spacing and 390 MeV meson mass. Figure 5 shows the effective anisotropy extracted from the ratio of spatial and temporal masses in the left panel and from the dispersion relation in the right panel.

We now introduce gauge links smearing in the quark operator on the anisotropic lattice. We hope for the same improvements, as it was the case on isotropic lattices: smeared link actions have improved chiral properties, renormalization constants are closer to the tree level values, so as the clover coefficient of the non-perturbative $O(a)$ -improvement. Additionally we expect, that the tuned bare quark anisotropy parameter $\xi_f^{(0)}$, for which $\xi_f = \xi_g$ holds, is closer to its tree level value, ie. to ξ_f .

The expectation is confirmed in a numerical experiment. We fix the bare fermion anisotropy to the gauge anisotropy, $\xi_f^{(0)} = \xi_g$, and study the renormalized fermion anisotropy for different number of “isotropic” stout smearing steps with parameters $\rho_{ij} = \rho_{i4} = \rho_{4i} = \rho$. In each case the pseudoscalar mass was tuned to $m_s = 0.25$ again. Figure 6 shows, that increasing the number of steps brings the fermion anisotropy closer to the gauge anisotropy, at four smearing steps their difference is less than 1%. This means that using this par-

ticular smearing, the tuning condition $\xi_f = \xi_g$ is satisfied to 1% precision without tuning the bare fermion anisotropy. The effect of changing the pseudoscalar mass by a factor two upwards is about on the level of the statistical error.

Interestingly as one increases the number of smearing steps beyond four, the fermion anisotropy decreases further and the tuning of the anisotropy parameter becomes necessary again (now in the other direction). “Isotropic” stout smearing washes out the anisotropy of the background gauge configuration.

This encourages us to consider stout smearing, with anisotropic parameters. A natural choice is to use the generator of the Wilson flow, ie. Equation (2.3) with coefficients $\rho_{i4} = \xi_g^2 \rho$ and $\rho_{ij} = \rho_{4i} = \rho$, as generator of the stout smearing transformation. There is however an important limitation. As it is known, stout smearing gets unstable for large smearing parameters. In our current numerical study we found, that the boundary of the instability region for the ρ parameter is reduced by a factor 3. In order to keep the strength of the smearing constant, we are forced to increase the number of smearing steps by the same factor. On Figure 6 we plot the results with this “anisotropic” stout smearing. As it can be seen it also brings the fermion anisotropy closer to the gauge anisotropy. Differently from the “isotropic” smearing, it does not get worse for larger number of smearing steps, the necessary tuning is getting gradually smaller as the number of smearing steps is increased.

Let us emphasize here, that the continuum limit is universal regardless of the details of the smearing in the Dirac operator. It is of practical importance to use a smearing, where the anisotropy renormalization is suppressed.

8 Parameter tuning with dynamical quarks

In this section we propose and test a strategy to tune the anisotropy parameters for $n_f = 3$ degenerate flavors of dynamical Wilson quarks.

As we have seen in the previous section, up to some precision there is no need to tune the bare fermion anisotropy, if the gauge link smearing in the Dirac operator is properly chosen. This can be achieved either by using “anisotropic” smearing with a high enough number of smearing steps. Or one can use “isotropic” smearing, it also reduces the necessary tuning until some number of smearing steps. In the latter case one has to be careful not to overdo the smearing. The bare fermion anisotropy $\xi_f^{(0)}$ is to be set to the target anisotropy. Only one anisotropy parameter, the bare gauge anisotropy $\xi_g^{(0)}$ has to be tuned until the renormalized gauge anisotropy ξ_g equals the target anisotropy.

We choose to use “isotropic” stout smearing in the Dirac operator to test the above strategy and take the same number of smearing steps, which has turned out to be optimal in the quenched case (ie. four steps with $\rho = 0.12$). We generated ensembles with tree level improved Symanzik gauge action and $n_f = 3$ flavors of dynamical Wilson quarks. The target anisotropy is 3, so we set $\xi_f^{(0)} = 3$. We use Rational Hybrid Monte Carlo algorithm combined with Hasenbusch preconditioning for the generation of configurations. The parameters which we use for the tuning are

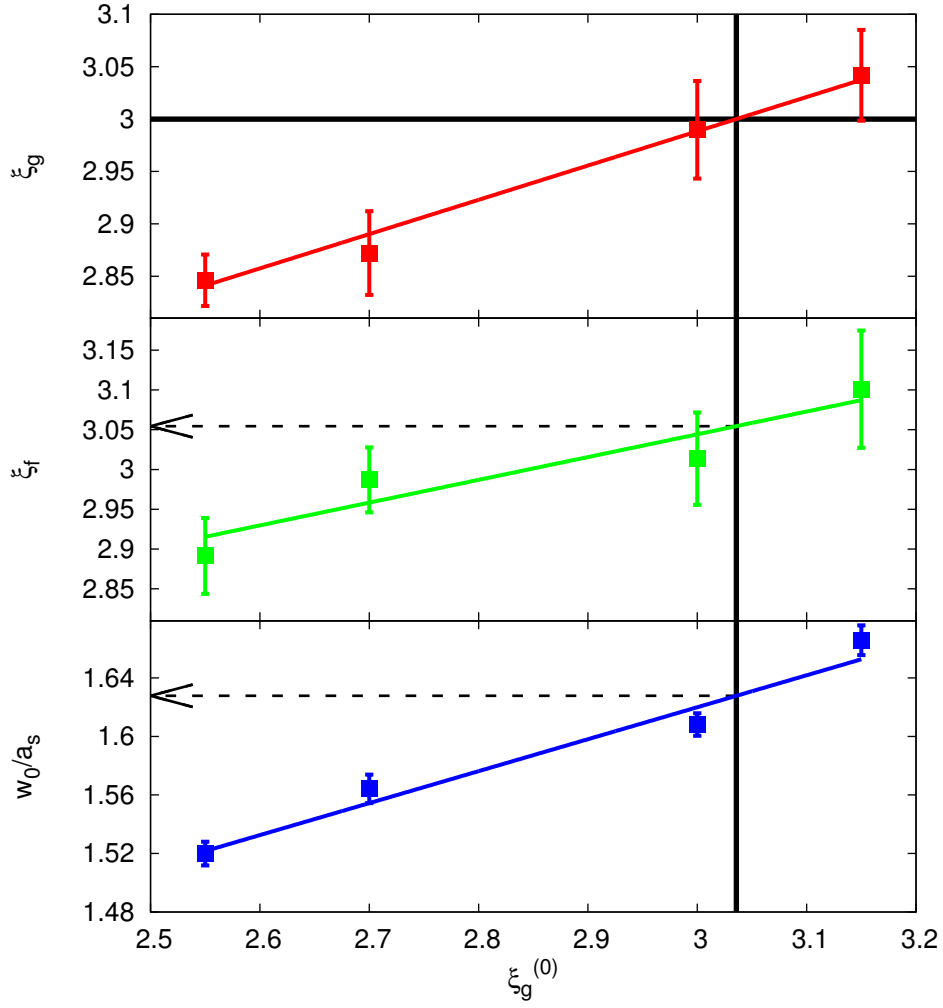


Figure 7. The gauge anisotropy, the fermion anisotropy and the w_0 -scale as the function of the bare gauge anisotropy in our runs with dynamical quarks.

lattice size	$16^3 \times 96$
β	3.5
m	-0.025
$\xi_f^{(0)}$	3.00
$\xi_g^{(0)}$	2.55, 2.70, 3.00, 3.15

On the upper panel of Figure 7 we plot the renormalized gauge anisotropy as function of the bare anisotropy in our four runs. The results can be interpolated by a linear fit. The gauge anisotropy takes the target value $\xi_g = 3$, when the bare anisotropy is set to $\xi_g^{(0)} = 3.04(x)$ ¹. At this parameter the fermion anisotropy is $\xi_f = 3.05(3)$, which is less than 2% and somewhat more than 1σ away from the desired point (where $\xi_f = \xi_g$). The

¹Suprisingly the bare and renormalized gauge anisotropies are consistent. It is most probably an accident, but it deserves more investigation.

w_0 -scale at this point is $w_0 = 1.63(3)$, this corresponds to a spatial lattice spacing of 0.11 fm. The pseudoscalar mass is 485 MeV.

We conclude that gauge link smearing also helps to decrease the fermion anisotropy renormalization in the dynamical case. In our concrete case no tuning of $\xi_f^{(0)}$ is needed, if the required precision is not better than 2%.

9 Conclusions

In this paper we generalized the w_0 scale to anisotropic lattices. We found that the scale setting procedure requires the knowledge of the anisotropy. We worked out a method to extract the renormalized anisotropy from the Wilson flow, which is also the basis of our scale setting. Our method is in agreement with the standard results based on ratios of Wilson loops, but does not rely on the interpolation of lattice data between lattice sites, nor does it require to evaluate large Wilson loops.

To illustrate the use of our measure for gauge anisotropy we tabulated the bare anisotropies of the tree-level Symanzik gauge action for three renormalized anisotropies. We also determined the scale setting w_0 and thus made the parameters available for immediate use.

We have studied the effect of smearing on the fermion anisotropy. We have observed on quenched configurations that both “isotropic” and “anisotropic” smearing significantly reduces the difference between the bare and renormalized anisotropy. This statement was also verified with three flavor dynamical simulations. In the future we will extend this study by determining the bare anisotropies with dynamical fermions for a wider range of lattice spacings and renormalized asymmetries.

A Lattice actions

The anisotropic gauge action is

$$\frac{\beta}{\xi_g^{(0)}} \sum_{x,i < j} \left[1 - \frac{1}{3} \text{Retr} \mathcal{U}_{ij}(x) \right] + \beta \xi_g^{(0)} \sum_{x,i} \left[1 - \frac{1}{3} \text{Retr} \mathcal{U}_{i4}(x) \right], \quad (\text{A.1})$$

where the $\mathcal{U}_{\mu\nu}(x)$ loop operator is constructed from gauge links along plaquettes and rectangles:

$$\mathcal{U}_{\mu\nu} = c_0 W_{\mu\nu}(1, 1) + c_1 W_{\mu\nu}(1, 2) + c_1 W_{\mu\nu}(2, 1). \quad (\text{A.2})$$

We use both the simple plaquette action $c_0 = 1, c_1 = 0$ and tree level Symanzik improved action $c_0 = 5/3, c_1 = -1/12$ in this paper.

We choose the anisotropic Wilson-clover Dirac operator as

$$\begin{aligned}
(D\psi)_x = & (m + 3 + \xi_f^{(0)})\psi_x - \\
& - \frac{\xi_f^{(0)}}{2} \left[(1 + \gamma_4)U_4(x)\psi_{x+i} + (1 - \gamma_4)U_4^\dagger(x-i)\psi_{x-i} \right] - \\
& - \frac{1}{2} \sum_i \left[(1 + \gamma_i)U_i(x)\psi_{x+i} + (1 - \gamma_i)U_i^\dagger(x-i)\psi_{x-i} \right] - \\
& - \frac{1}{2} \sum_{i>j} c_s^{SW} f_{ij}(x) \sigma_{ij} \psi_x - \frac{1}{2} \sum_i c_t^{SW} f_{4i}(x) \sigma_{4i} \psi_x,
\end{aligned} \tag{A.3}$$

where the Dirac-sigma matrices are $\sigma_{\mu\nu} = 1/2[\gamma_\mu, \gamma_\nu]$ and the $f_{\mu\nu}(x)$ loop operator is the discretization of the field-strength tensor built up from gauge links along the clover path. For the clover coefficients we choose $c_s^{SW} = 1$ and $c_t^{SW} = (\xi_f^{(0)} + 1)/2$. Our definition is very similar to that of Reference [12], the difference is, that they use $c_t^{SW} = (\xi_g^{(0)}/\xi_f^{(0)} + \xi^*)/2$, where ξ^* is the target anisotropy.

Acknowledgments

We thank Christian Hoelbling for useful discussions. This research has been partly supported by the European Research Council grant 208740 (FP7/2007-2013). Computations were performed on the Blue Gene supercomputers at FZ Jülich on the QPACE facility supported by the Sonderforschungsbereich TR55 and on GPU [27] clusters at the Wuppertal University.

References

- [1] S. Durr, Z. Fodor, J. Frison, C. Hoelbling, R. Hoffmann, *et al.*, *Ab-Initio Determination of Light Hadron Masses*, *Science* **322** (2008) 1224–1227, [[0906.3599](#)].
- [2] N. Mathur, Y. Chen, S. Dong, T. Draper, I. Horvath, *et al.*, *Roper resonance and $S(11)(1535)$ from lattice QCD*, *Phys.Lett.* **B605** (2005) 137–143, [[hep-ph/0306199](#)].
- [3] **CSSM Lattice collaboration** Collaboration, M. S. Mahbub, W. Kamleh, D. B. Leinweber, P. J. Moran, and A. G. Williams, *Roper Resonance in 2+1 Flavor QCD*, *Phys.Lett.* **B707** (2012) 389–393, [[1011.5724](#)]. 7 pages, 5 figures. Revised version with new results to appear in PLB.
- [4] C. J. Morningstar and M. J. Peardon, *The Glueball spectrum from an anisotropic lattice study*, *Phys.Rev.* **D60** (1999) 034509, [[hep-lat/9901004](#)].
- [5] **CP-PACS Collaboration** Collaboration, T. Manke *et al.*, *Hybrid quarkonia on asymmetric lattices*, *Phys.Rev.Lett.* **82** (1999) 4396–4399, [[hep-lat/9812017](#)].
- [6] J. Harada, H. Matsufuru, T. Onogi, and A. Sugita, *Heavy quark action on the anisotropic lattice*, *Phys.Rev.* **D66** (2002) 014509, [[hep-lat/0203025](#)].
- [7] P. Chen, *Heavy quarks on anisotropic lattices: The Charmonium spectrum*, *Phys.Rev.* **D64** (2001) 034509, [[hep-lat/0006019](#)].

- [8] **CP-PACS Collaboration** Collaboration, M. Okamoto *et al.*, *Charmonium spectrum from quenched anisotropic lattice QCD*, *Phys.Rev.* **D65** (2002) 094508, [[hep-lat/0112020](#)].
- [9] T. R. Klassen, *The Anisotropic Wilson gauge action*, *Nucl.Phys.* **B533** (1998) 557–575, [[hep-lat/9803010](#)].
- [10] **CP-PACS Collaboration** Collaboration, T. Umeda *et al.*, *Two flavors of dynamical quarks on anisotropic lattices*, *Phys.Rev.* **D68** (2003) 034503, [[hep-lat/0302024](#)].
- [11] R. Morrin, A. O. Cais, M. Peardon, S. M. Ryan, and J.-I. Skullerud, *Dynamical QCD simulations on anisotropic lattices*, *Phys.Rev.* **D74** (2006) 014505, [[hep-lat/0604021](#)].
- [12] R. G. Edwards, B. Joo, and H.-W. Lin, *Tuning for Three-flavors of Anisotropic Clover Fermions with Stout-link Smearing*, *Phys.Rev.* **D78** (2008) 054501, [[0803.3960](#)]. 23 pages, 18 figures.
- [13] **Hadron Spectrum Collaboration** Collaboration, H.-W. Lin *et al.*, *First results from 2+1 dynamical quark flavors on an anisotropic lattice: Light-hadron spectroscopy and setting the strange-quark mass*, *Phys.Rev.* **D79** (2009) 034502, [[0810.3588](#)].
- [14] L. Liu, G. Moir, M. Peardon, S. M. Ryan, C. E. Thomas, *et al.*, *Excited and exotic charmonium spectroscopy from lattice QCD*, [1204.5425](#).
- [15] G. Aarts, C. Allton, M. B. Oktay, M. Peardon, and J.-I. Skullerud, *Charmonium at high temperature in two-flavor QCD*, *Phys.Rev.* **D76** (2007) 094513, [[0705.2198](#)].
- [16] S. Durr, Z. Fodor, C. Hoelbling, S. Katz, S. Krieg, *et al.*, *Lattice QCD at the physical point: light quark masses*, *Phys.Lett.* **B701** (2011) 265–268, [[1011.2403](#)].
- [17] S. Durr, Z. Fodor, C. Hoelbling, S. Katz, S. Krieg, *et al.*, *Lattice QCD at the physical point: Simulation and analysis details*, *JHEP* **1108** (2011) 148, [[1011.2711](#)].
- [18] S. Borsanyi, S. Durr, Z. Fodor, C. Hoelbling, S. Katz, *et al.*, *QCD thermodynamics with continuum extrapolated Wilson fermions I*, . 15 pages, 9 figures.
- [19] M. Luscher and P. Weisz, *Perturbative analysis of the gradient flow in non-abelian gauge theories*, *JHEP* **1102** (2011) 051, [[1101.0963](#)]. Plain TeX source, 28 pages, 14 figures/ v2: typos corrected, agrees with published version.
- [20] M. Luscher, *Trivializing maps, the Wilson flow and the HMC algorithm*, *Commun.Math.Phys.* **293** (2010) 899–919, [[0907.5491](#)].
- [21] R. Narayanan and H. Neuberger, *Infinite N phase transitions in continuum Wilson loop operators*, *JHEP* **0603** (2006) 064, [[hep-th/0601210](#)].
- [22] C. Morningstar and M. J. Peardon, *Analytic smearing of SU(3) link variables in lattice QCD*, *Phys.Rev.* **D69** (2004) 054501, [[hep-lat/0311018](#)].
- [23] M. Luscher, *Properties and uses of the Wilson flow in lattice QCD*, *JHEP* **1008** (2010) 071, [[1006.4518](#)].
- [24] S. Borsanyi, S. Durr, Z. Fodor, C. Hoelbling, S. D. Katz, *et al.*, *High-precision scale setting in lattice QCD*, [1203.4469](#). 15 pages, 7 figures, 2 tables.
- [25] S. Sakai, T. Saito, and A. Nakamura, *Anisotropic lattice with improved gauge actions. 1. Study of fundamental parameters in weak coupling regions*, *Nucl.Phys.* **B584** (2000) 528–542, [[hep-lat/0002029](#)].
- [26] S. Sakai and A. Nakamura, *Improved gauge action on an anisotropic lattice. 2. Anisotropy parameter in the medium coupling region*, *Phys.Rev.* **D69** (2004) 114504, [[hep-lat/0311020](#)].

- [27] G. I. Egri, Z. Fodor, C. Hoelbling, S. D. Katz, D. Nogradi, *et al.*, *Lattice QCD as a video game*, *Comput.Phys.Commun.* **177** (2007) 631–639, [[hep-lat/0611022](#)].

β	$\xi_g = 1$		$\xi_g = 2$		$\xi_g = 3$		$\xi_g = 4$	
	w_0		w_0	ξ_0	w_0	ξ_0	w_0	ξ_0
4.20	1.2607(3)	1.0000(6)	1.8070(31)	1.8070(31)	0.9340(1)	2.6415(7)	0.8527(2)	3.4380(28)
4.30	1.4851(3)	1.1823(3)	1.8205(14)	1.8205(14)	1.0671(10)	2.6513(47)	1.0153(5)	3.4851(37)
4.46	1.8877(14)	1.5199(6)	1.8293(14)	1.8293(14)	1.3814(6)	2.6714(21)	1.3188(6)	3.5221(31)
4.60	2.3002(22)	1.8612(16)	1.8386(32)	1.8386(32)	1.6946(6)	2.6880(51)	1.6242(19)	3.5480(70)
4.70	2.6211(24)	2.1409(27)	1.8461(22)	1.8461(22)	1.9540(20)	2.6899(49)	1.8721(30)	3.5699(109)
4.81	3.0295(34)	2.4779(49)	1.8457(56)	1.8457(56)	2.2708(28)	2.7102(42)	2.1690(59)	3.5685(122)
4.90	3.4200(98)	2.7945(54)	1.8554(35)	1.8554(35)	2.5531(32)	2.7273(94)	2.4511(48)	3.5799(121)
5.00	3.8830(137)	3.1732(112)	1.8554(92)	1.8554(92)	2.9163(39)	2.7319(105)	2.7974(53)	3.5890(108)
5.10	4.3727(242)	3.5886(112)	1.8649(143)	1.8649(143)	3.3482(67)	2.7461(87)	3.2122(75)	3.6144(166)
5.20	4.9609(498)	-	-	-	3.8628(200)	2.7460(115)	3.6359(148)	3.6016(302)

Table 2. The scale and bare anisotropy at various gauge couplings and target anisotropies of the tree-level Symanzik gauge action. In this action we keep the (1x2) rectangles in all orientations, thus with $\xi_0 = 1$ the isotropy is completely restored. For comparison and other possible uses we give the w_0 scale on isotropic lattices, as well.